IEEE Access
Multidisciplinary | Rapid Review | Open Access Journal

Received October 31, 2019, accepted November 13, 2019, date of publication November 18, 2019, date of current version December 4, 2019.

Digital Object Identifier 10.1109/ACCESS.2019.2953960

Evaluation of DC-Subway Stray Current Corrosion With Integrated Multi-Physical Modeling and Electrochemical Analysis

ZHICHAO CAI[1,2], XIANWEI ZHANG[1], AND HAO CHENG[1]

[1]School of Electrical and Automation Engineering, East China Jiaotong University, Nanchang 330013, China
[2]Nondestructive Detection and Monitoring Technology for High Speed Transportation Facilities, Key Laboratory of Ministry of Industry and Information Technology, Nanjing 211106, China

Corresponding author: Zhichao Cai (czchebut@foxmail.com)

This work was supported by the National Natural Science Foundation of China under Grant 51807065.

ABSTRACT Leakage of stray current can cause serious problems by accelerating the corrosion process of a buried pipeline in the subway. A multi-physical finite element model of the DC-subway traction system was established in this study, and the dynamic process of the stray current corrosion on buried pipeline was calculated according to the real time traction conditions. In this study, the corrosion rate variation of stray current is evaluated, and the corrosion trend of stray current is quantitatively calculated. The model simulation shows that the stray current corrosion is significantly higher than other processes during the acceleration process of the subway locomotive. And the potential of the buried pipeline reaches a maximum value when an up-rush of traction current occurs. The corrosion is mainly concentrated in the anode region of the buried pipeline, and the closer the buried pipeline is to the rail the more serious the corrosion is. A corrosion experiment of N20 carbon steel was carried out and verified by finite element model. The results further show that the finite element model can quantitatively calculate and predict the mass loss of buried metal caused by stray current corrosion.

INDEX TERMS Corrosion, DC-subway, finite element method, stray current.

I. INTRODUCTION

With the advancement of urbanization, traffic congestion is widespread in large and medium-sized cities. The subway system has become widely used as a convenient and clean transportation in various cities to ease traffic pressure. In the subway system as seen in Fig. 1, a power circuit of subway vehicles is formed by DC traction substations, overhead catenary system, and return-flow system. However, the rail cannot be completely insulated from the earth as a return conductor, and part of the return current flowing through the rail will leak to the earth, which becomes stray current [1], [2]. In the process of stray current flow into buried metallic structure before returning to the negative of the substation, the buried metal is electrolyzed due to the electrochemical corrosion. Stray current corrosion reduces the life of the buried metal such as pipelines. In the United States and the United Kingdom the infrastructure damage loss and repair costs due to stray current corrosion are as high as $500-700 million per annum [3], [4]. In order to effectively prevent the damage caused by stray current, researches are carried out based on several aspects such as reducing stray current leakage and establishing prediction models of the distribution of stray current.

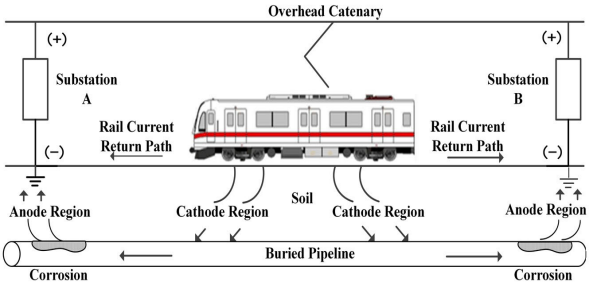

FIGURE 1. Stray current corrosion on buried pipeline.

Many studies have shown that some measures can be taken to minimize the effects of stray current, such as increasing rail-to-ground resistance and system rated voltage, reducing

The associate editor coordinating the review of this manuscript and approving it for publication was Su Yan.

rail resistance and substation distance, performing stray current collection, using protection of cathode, using insulating mats, etc [5]–[8]. The magnitude of the stray current is determined by the operating conditions of the subway locomotive. Generally, the stray current increases with the increase of the traction current during the traction acceleration or braking phase of the train [9], [10]. In addition, the difference in grounding mode will also change the distribution of stray current. In the prevention of stray current, the corresponding grounding method should be adopted according to the actual situation of the subway line [11]–[13]. Measuring and controlling stray current is difficult because of the complex condition of an actual DC-subway system. Therefore, experts have attempted to establish models of subway system to analyze the distribution of stray current.

At present, a large number of analytical models focus on the distribution of stray current, such as resistance network models, electric field models, potential gradient models and hemispherical electrode models [14]–[18]. With the deepening of research, simulation software such as Simulink, CEDGS, and FEM software are also widely used to study the distribution of stray current [1], [19]–[22]. By comparison with the traditional models, the simulation models can reduce oversimplification, which provide effective tools for analyzing the distribution of stray current under complex environmental conditions. The above models provide effective tools for analyzing the leakage and distribution of stray current. However, the study of the distribution of stray current is only the beginning of stray current corrosion analysis. It will be more instructive for preventing and controlling stray currents, if a model for directly calculating stray current corrosion of buried metals can be established.

In this paper, the proposed multi-physical FEM Model can simulate the dynamic distribution of the stray current in the subway. And the FEM model can quantitatively calculate the metal corrosion in the area affected by the stray current. The FEM model provides a new analysis tool for solving the stray current problem, which will also greatly improve the efficiency of stray current control. The rest of the paper is organized as follows. Section II provides details regarding the subway system and load condition. The dynamic FEM modeling process and simulation results based on the moving conditions of the subway locomotive are introduced in Sections III and IV, respectively. Finally, the N20 carbon steel experiment simulating stray current corrosion and the corresponding three-dimensional FEM model are discussed in Section V.

II. SYSTEM AND LOAD CONDITION DESCRIPTION

The most common locomotive of Guangzhou Metro comprises three basic types of vehicles, namely Tc, M_P and M. Six vehicles are grouped together, as shown in Fig. 2. The locomotive formation type (–Tc* M_P^* M = M * M_P^* Tc–), the letters Tc, M_P and M represent the locomotive's motor car, trailer and the car without pantograph respectively. A motor car has 4 DC motors; Thus, the entire locomotive has

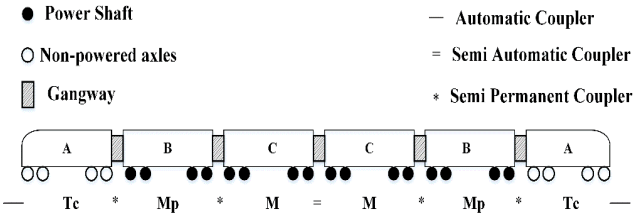

FIGURE 2. Train formation of Guangzhou Metro.

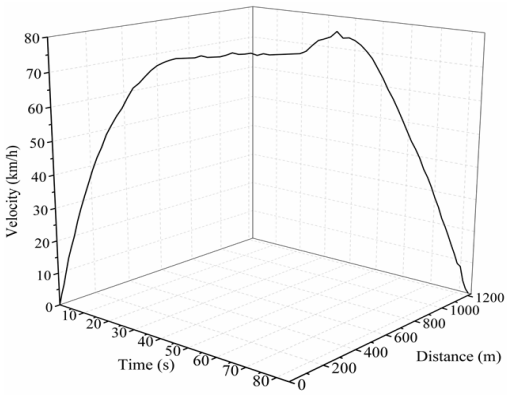

FIGURE 3. Velocity and distance curves from Shibi station to Huijiang station.

16 parallel DC motors. All of these motors are in the operation model and provide traction power. In order to facilitate the calculation, 16 parallel excitation sources can be reduced to a single large traction source in the finite element model.

The simulation of stray current is usually based on one interval of the subway, as the locomotive's traction characteristics remained similar at each interval. So this study focuses on the traction characteristics from Shibi Station to Huijiang Station through a field test of Guangzhou Metro, which can represent the busiest time with the maximum load. The locomotive was tested from Shibi Station to Huijiang Station for a total of 84s, and the velocity of running locomotive is a time-varying process. The speed sensor in the locomotive collects the speed every 0.1 seconds. We can assume that the distance of the locomotive running at one time is S_n and the velocity at this moment is V_n. After time Δt (0.1s), the distance of the locomotive running becomes S_{n+1} and V_{n+1} at the moment. The distance calculation equation of the locomotive is shown as follows, and the velocity and distance of the locomotive are presented in Fig. 3.

$$\begin{cases} a_n = (V_{n+1} - V_n)/\Delta t \\ S_{n+1} = S_n + \dfrac{V_{n+1}^2 - V_n^2}{2a_n} \end{cases} \tag{1}$$

$$S_{total} = \sum_{i=1}^{m} S_n \tag{2}$$

where a_n is an accelerated velocity the at one time, m is the total number of velocities in one interval, S_{total} is the total displacement in one interval.

Fig. 3 also shows three different modes of operation for the locomotive: acceleration, constant-speed and deceleration. The locomotive leaves the Shibi station in an accelerated

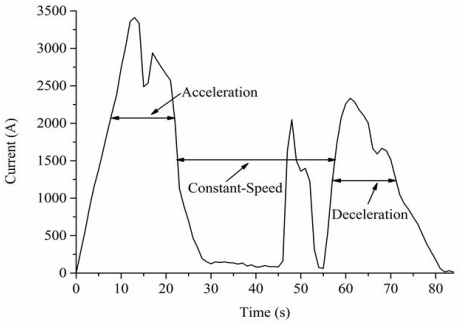

FIGURE 4. Traction current of a locomotive from Shibi station to Huijiang station.

manner and runs for 24 seconds before entering the constant-speed phase. Then the locomotive kept moving at a high velocity, and enters the deceleration phase at 52s, then the locomotive stops at Huijiang Station at 84s. The traction current directly determines the traction force or braking force, which affects the acceleration and deceleration of the locomotive, therefore, traction current has obvious time correspondence with locomotive velocity, which can be seen in Fig. 4. The traction current has an upward rush when the locomotive runs to 48s. It is possible that the locomotive encounters different paths, such as uphill, downhill and curved, and the traction current changes to ensure that the speed is maintained in a stable range when the locomotive is running uniformly.

III. DYNAMIC FEM MODEL DESCRIPTION

A. GEOMETRIC MODEL

As shown in Fig. 5, a geometric model from Shibi Station to Huijiang Station was established, which includes locomotive, stations, rail, soil and buried pipeline. In this model, a dynamic locomotive, whose traction current and velocities are taken from the data in Section 2, is moving from Shibi Station to Huijiang Station. The lower surface of the locomotive serves as the input current boundary, and the lower surface of the stations are grounded. Under the above conditions, a stray current distribution field is formed in the soil, which provides an electrochemical corrosion environment for the buried pipeline metal.

B. PHYSICAL MODEL

In the geometric model, a current field is formed in the soil due to the leakage of stray current. In the soil, the soil conductivity determines the size and distribution of stray current, assuming that the influence of other factors is not considered. With the distribution of stray current in the soil (electrolyte), different potential layers will form in the soil. According to the constant electric field theory, the electrolyte (soil) potential ϕ_l can be solved according to the Laplace's equation (3), and the current density in the soil is governed by the Ohm's law as equation (4):

$$\nabla^2 \phi_l = 0 \tag{3}$$

$$i_l = -\sigma_l \nabla \phi_l \tag{4}$$

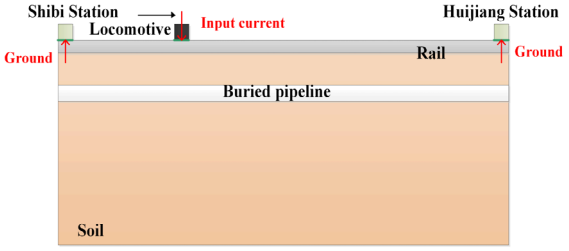

FIGURE 5. Schematic of finite element model.

In equation (4), i_l represents the current density, σ_l is the soil conductivity.

In the stray current field, as shown in Fig. 5, the buried pipeline metal, soil electrolyte and current loop constitute the basic elements of the electrochemical cell. Some of the stray current distributed in the soil flows back to the ground through the soil directly. The other part flows through the buried pipeline metal firstly, and then returns to the ground. The model mainly studies the overall corrosion effect of the buried pipeline in the stray current field, so the whole buried pipeline metal is defined as the anode. The moving locomotive is defined as the cathode to assist the model calculation. The specific electrochemical reaction equations and the principle of substance transfer involved in the electrochemical reaction are as follows:

Cathode reaction: $O_2 + 2H_2O + 4e^{-1} = 4OH^{-1}$

And the Oxygen transport is controlled by the Fickian diffusion equation:

$$\nabla \cdot D_{O2}(\nabla C_{O2}) = 0 \tag{5}$$

where D_{O2} is the diffusion coefficient of the oxygen and C_{O2} is the oxygen concentration.

Anode reaction: $Fe = Fe^{2+} + 2e^{-1}$

The anode region loses electrons and becomes ferrous ions dissolved in the soil. In the electrolyte, the electrode over potential η is calculated from:

$$\eta = \phi_s - \phi_l - E_{eq,m} \tag{6}$$

where ϕ_s is the potential of the electrode, ϕ_l is the potential of electrolyte and $E_{eq,m}$ is the equilibrium potential electrode reaction. The electrode reaction can be expressed by Tafel's kinetics.

The current density for the oxygen reduction is:

$$i_{O2} = \left(\frac{c}{c_{ref}}\right) i_{0,O2} 10^{\frac{\eta_{O2}}{A_{O2}}} \tag{7}$$

The current density for the iron reaction i_{Fe} is:

$$i_{Fe} = \left(\frac{c}{c_{ref}}\right) i_{0,Fe} 10^{\frac{\eta_{Fe}}{A_{Fe}}} \tag{8}$$

where i_{O2} and i_{Fe} are reduction current density, c_{ref} is the pipeline-concrete interfacial concentration, $i_{0,O2}$ and $i_{0,Fe}$ are the exchange current density, A_{O2} and A_{Fe} are the Tafel slope.

The dissolution of iron metal causes a decrease in velocity according to:

$$v = \frac{M}{nF} i_{Fe} \tag{9}$$

TABLE 1. Parameters of electrochemical reaction.

Parameters	Value	Unit	Description
$E_{eq,Fe}$	- 0.76	V	Iron equilibrium potential
$E_{eq,O2}$	1.23	V	Oxygen equilibrium potential
$i_{0,Fe}$	7.1E-5	A/m^2	Iron exchange current density
$i_{0,O2}$	1E-8	A/m^2	Oxygen exchange current density
A_{Fe}	0.41	mV/dec	Iron ion Reduction Tafel Slope
A_{O2}	-0.25	mV/dec	Oxygen ion Reduction Tafel Slope
D_{O2}	1E-7	m^2/s	Oxygen diffusion coefficient
C_{O2}	0.2	mol/m^3	Initial oxygen ion concentration
M	56	g/mol	Average molar mass of iron
n	2		Iron electrons lost
σ_{Fe}	1E7	S/m	Electrolyte conductivity of the pipeline metal
σ_l	0.01	S/m	Electrolyte conductivity of the soil
F	96485	C/mol	Faraday constant

where M is the average molar mass of iron, n is the number of electrons lost by the iron reaction, and F is the Faraday constant.

C. NUMERICAL ALGORITHM

The model is calculated by finite element software COMSOL Multiphysics. The COMSOL software itself sets up multiple physical-field modules. In this research model, the physical-fields used to calculate the stray current corrosion of buried metal include DC current field, secondary current distribution and transport of diluted species in electrochemical module. The parameters involved in the electrochemical module during the modeling process are shown in Table 1.

In the finite element model, meshing is an important part of the accuracy of simulation calculation. In order to accurately resolve the dynamic distribution of stray currents between the rail and soil because of locomotive movement, adaptive meshing is used. This means that as the interface moves during the simulation, the mesh is updated in order to keep the mesh refined in the interface region. The geometric dimensions of the dynamic model in this paper are shown in Table 2, and the results of dynamic meshing are shown in Fig. 6. In order to make the shape of the model more coordinated, some geometrical dimensions, which do not affect the simulation results, are not set according to actual parameters such as stations and locomotive. The division of the mesh is achieved by the mapping method and the completed meshes consist mesh vertices of 15902, quadrilateral elements of 15522, edge elements of 1938 and 36 vertex elements, the total elements number is equal to quadrilateral elements.

IV. RESULTS AND DISCUSSION

The system is simulated in the above FEM model, as shown in Fig. 7. The rail is dark red colour, which indicates the current density in the rail is very high, as well as indicates that the rail is the main way for traction current to return to the substations of adjacent stations. Since the rail is not insulated

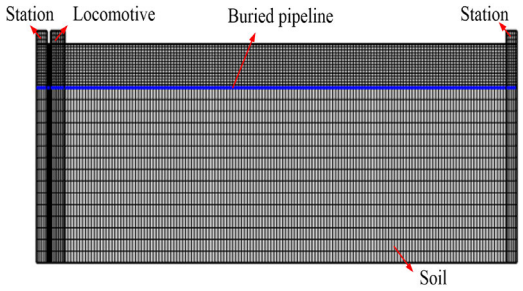

FIGURE 6. Mesh results.

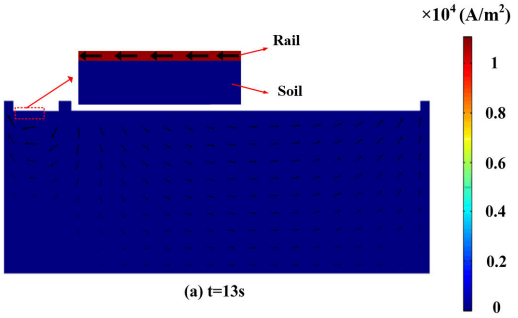

FIGURE 7. The distribution of electric current in rail and soil.

TABLE 2. Parameters of electrochemical reaction.

Geometric Parameters	Value
Soil length	1500 m
Soil height	500 m
Metal thickness of buried pipe	5 cm
Station Length	100 m
Station Height	30 m
Locomotive Length	40 m
Locomotive Height	30 m
Initial position of the locomotive	10 m
Rail height	18 cm

from the soil, some current (stray current) leaks into the soil. The navy blue colour of the soil indicates that the current density in the soil is very low.

In Fig. 4, the traction current is changing with the conditions of the locomotive, and the maximum value of the traction current appears at 13s in the acceleration phase and 61s in the deceleration phase. The distribution of stray current of the locomotive running to 13s and 61s is shown in Fig. 8. We can see from Fig. 8 that the stray current leakage of the locomotive shows a large value at these two moments by adjusting the current density scale of the FEM model. And it means that the nearby metal structures, including rail and buried pipeline, are vulnerable to corrosion. The stray current field in the soil forms a current density on the buried pipeline. And the current density distribution characteristics are closely related to the traction current of the locomotive. The heavily corroded area of the buried pipeline will also appear in the area where the traction current value of the locomotive is relatively high.

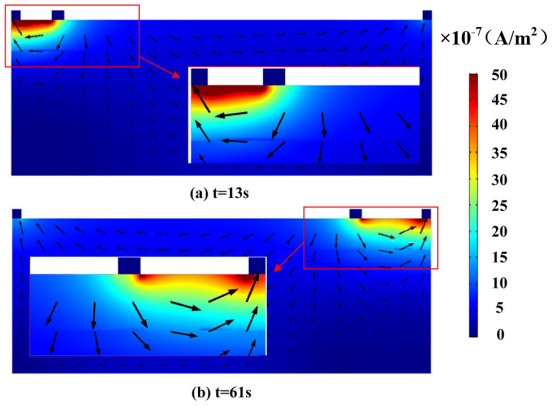

FIGURE 8. Stray current distribution in the soil.

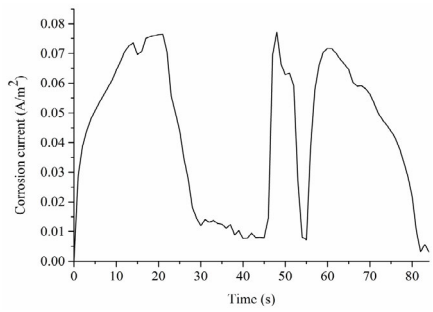

FIGURE 9. Corrosion current density of buried pipeline.

The current density distribution across the buried pipeline can be plotted as a graph by a dynamic model, which can be seen in Fig. 9. When the locomotive has a certain traction current loading (acceleration, deceleration), that is, there is a significant stray current leakage and corrosion phenomenon, the corrosion rate is mainly related to the traction current amplitude. Compared with the traction current (Fig. 4), the current density of metal exhibits the same trend, which fully demonstrates that the traction current determines the current flowing through the buried pipeline. In other words, the operating conditions of the locomotive directly affect the corrosion of the buried pipeline.

The traction current of the locomotive determines the distribution of stray current in the soil and the corrosion of the buried pipeline, and the greater the traction current is, the more serious the corrosion of the buried pipeline is.

Based on the stray current density on the buried pipeline and the electrochemical corrosion theory, the corrosion rate of the buried pipeline metal (anode) can be calculated by the FEM dynamic model. Fig. 10 is a three-dimensional view showing the corrosion rates of buried pipelines with different depth as a function of time and train location, where the color indicates the value of the corrosion rate of the buried pipeline. Comparing Fig. 10 (a), (b) and (c), the corrosion rates of three different buried pipelines (H = 50m, H = 100m, H = 150m), some conclusions can be drawn: Firstly, the corrosion trend of stray current is consistent; Secondly, serious corrosion occurs at both ends of the buried pipeline (large traction current

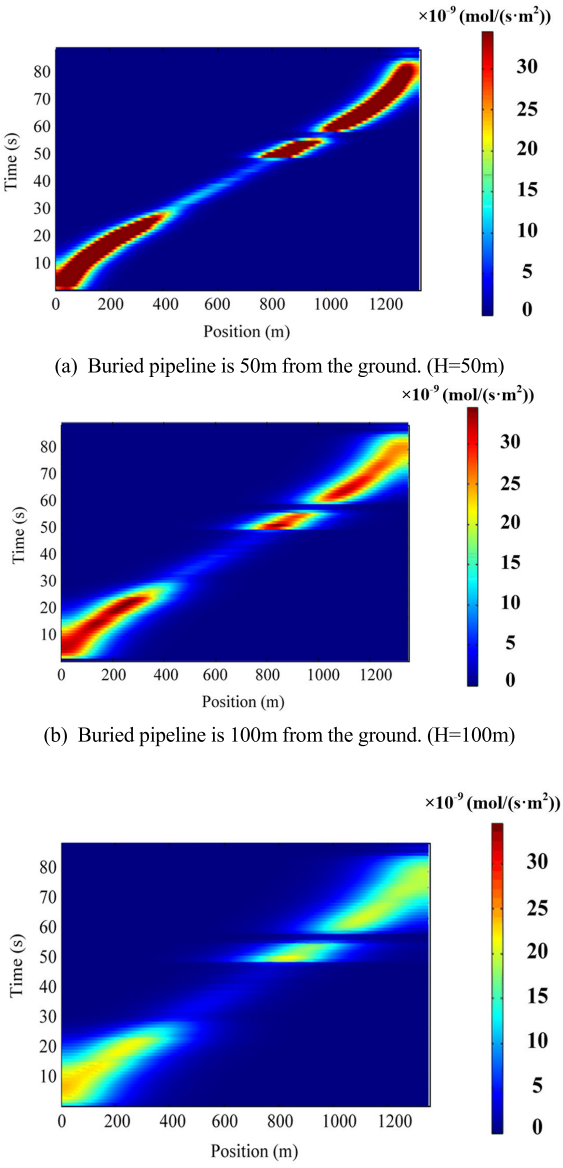

FIGURE 10. 3D plot of total corrosion rate.

regions); Thirdly, the deeper the buried pipeline is, the lower the corrosion rate will be.

FEM model provides powerful computing tools, and the overall corrosion rate of the pipeline can be got by surface integral operation. As shown in Fig. 11, the variation curves of the cumulative corrosion mass loss of the buried pipeline metal with time can be obtained while the overall corrosion rates of the pipelines multiplied by the running time of the locomotive. The slope in the figure indicates that the mass of corrosion loss of the buried pipeline increases rapidly when the locomotive starts to accelerate. When the locomotive is in the constant-speed mode, the corrosion mass increases slowly; when the locomotive enters the braking phase, the corrosion mass increases again rapidly. The corrosion mass loss can be used as an important criterion for predicting the degree of corrosion.

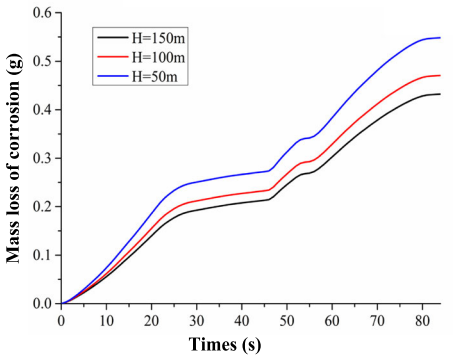

FIGURE 11. Corrosive mass loss of buried pipeline.

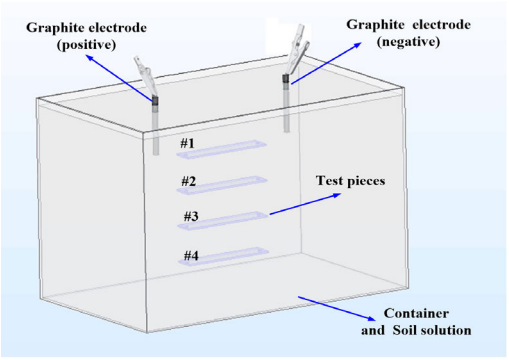

FIGURE 12. Electrochemical corrosion experimental system for stray current.

TABLE 3. Meterial composition of the solution.

Parameters	Na_2SO_4	NaCl	$NaHCO_3$	Distiled water
Value	150 g	300 g	50 g	0.021 L

V. EXPERIMENT AND SIMULATION VERIFICATION

A. SPECIMEN AND SOLUTION

To further illustrate the accuracy of the above integrated multi-physical model for the assessment of stray current corrosion and the local corrosion effects of buried metal, an experimental platform was designed to simulate the experimental environment of stray current corrosion of buried metals, as shown in Fig. 12. The test pieces used in the experiment were made of N20 carbon steel and were made to test pieces of 120mm in length, 25mm in width, and 2mm in thickness. In the experiment, the salt in the soil was expressed by Na_2SO_4, NaCl and $NaHCO_3$, and the mass ratio was 3:6:1. These three components in the above ratio were gradually placed in a container with distilled water until the solution obtained the conductivity required for the experiment. As seen in the Fig. 12, the test pieces of #1, #2, #3, #4 were placed at different depths of the solution, and the two graphite electrodes were respectively connected to the positive and negative electrodes of the DC power supply to realize an electric field applied to the solution. An environment of stray current distribution was created, the positive graphite electrode is the leakage point of the stray current, and the negative graphite electrode represents the stray current reflow point.

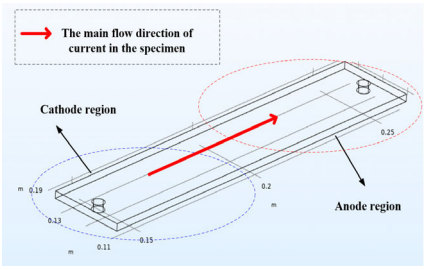

(a) Distribution of test piece electrodes

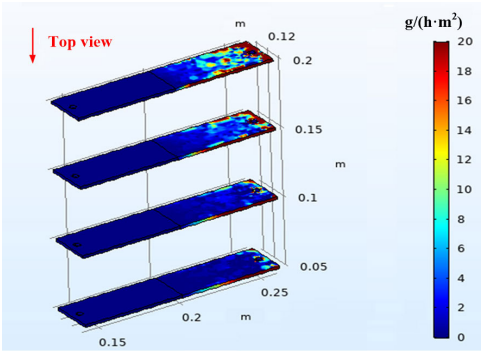

(b) Simulation of corrosion rate

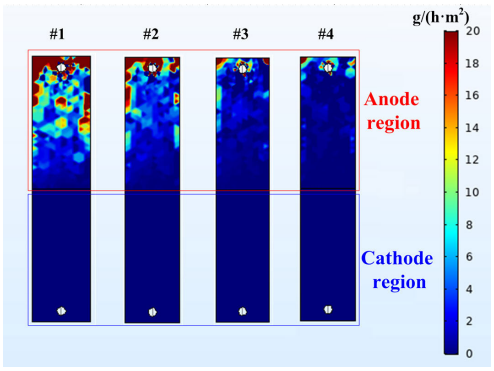

(c) Corrosion rate (Top view)

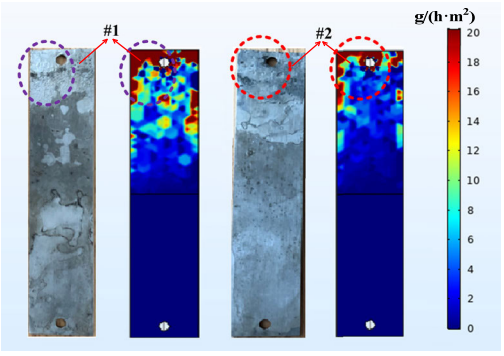

(d) Contrast graph (top view)

FIGURE 13. Simulation and experimental results.

B. ELECTROCHEMICAL CORROSION

In order to obtain the electrochemical corrosion effect of the test pieces faster, the conductivity of the solution was set to

TABLE 4. Experimental and simulation data.

Depth (mm)	Pre-test mass（g）	Post-test mass（g）	Text corrosion mass（g）	Text corrosion rate（g/h）	Simulated corrosion mass（g）	Simulated corrosion rate（g/h）
50	39.95	37.20	2.75	0.0550	2.88	0.0580
100	39.99	38.43	1.56	0.0312	1.53	0.0302
150	40.02	39.17	0.85	0.0170	0.81	0.0159
200	40.04	39.41	0.63	0.0126	0.61	0.0133

3 S/m during the experiment. The experiment was used to test the corrosion of different depths of test pieces weighed before and after the test. The test pieces were weighed before the experiment and the weight data was recorded. The applied voltage was 15V, and the power-on time was 50 hours. After the experiment, the corrosion test pieces were cleaned and dried, and then re-weighed. The material composition of the solution is shown in Table 3.

C. CORROSION ANALYSIS AND WEIGHT LOSS MEASUREMENT

A 1:1 three-dimensional FEM model was built according to the experimental platform, and the main parameters of the electrochemical reaction in the model are shown in Table 1. Unlike the above dynamic model, in the three-dimensional model, the voltage applied by the model is constant, which can be understood as the stray current leakage of the locomotive at a certain location. In addition, in the three-dimensional model, the stray current in the simulation is distributed three-dimensionally, and the cathode as well as the anode appears in the sample itself in the solution. In the three-dimensional model, we cannot perform electrode division like the two-dimensional model. In order to accurately reflect the actual experiment, the electrode boundary must be applied to the test piece during the simulation, as shown in Fig. 13(a). The depths of the #1 to #4 test pieces in the solution are 50mm, 100mm, 150mm and 200mm, respectively. The 3D FEM model can simulate the size distribution of the surface corrosion rate of the test piece as shown in Fig. 13(b). The mass of the test pieces lost can be obtained by surface integral operation results multiplied by the corrosion time.

There are following three conclusions can be drawn from Fig. 13(c) :

1) The closer to the cathode, the lower the corrosion rate;

2) The corrosion of the surface of the test piece is uneven and local;

3) The buried depth of the test pieces is inversely proportional to the corrosion rate. The deeper the burial depth is, the smaller the corrosion rate is;

In Fig. 13(d), comparing the experimental corrosion diagram and simulation diagram of two test pieces with depth of 50mm and 100mm respectively, what can be seen is that the corrosion area of the test pieces is also concentrated in the anode area, the cathode area is rarely corroded in the experiment. In addition, comparing two test pieces with different depths, the test piece with a depth of 50mm in the experiment is more corrosive than the test piece with a depth of 100mm, which can be seen from the local details of the upper left corners of the pieces. At the same time, it can be found that the simulation results can accurately reflect the electrochemical corrosion law: the current flows out from the anode surfaces of the test pieces, and the current density of the upper surfaces and the side surfaces is larger, so the corrosion is more serious. Generally, the corrosion rate of the anode region of the test piece is high and the center is low, and what can be seen in the Fig. 13(d) is that the area with high corrosion rate in the simulation diagram is the most severely corroded area of the experimental pieces.

The simulation model calculates the corrosion rate (v) of each point on the surface of the test piece by reference to (9). The overall corrosion rate of the test piece is obtained by integrating the corrosion rate at each point on the surface of the test piece, and the quality of the specimen being corroded can be obtained by multiplying the corrosion time. The experimental data and simulation data are shown in Table 4.

Due to the limitations of the conditions, experimental errors will inevitably occur during the experiment. For example, the dynamic changes of parameters such as solution concentration and conductivity during the experiment, metal secondary oxidation problems, etc. will also affect the corrosion results to some extent. Therefore, it is an objective reality that the simulation results and the experimental results cannot be completely consistent. But, by analyzing the results, it is not difficult to find out that the corrosion rate error is not more than 5% through the data in Tab. 2, which is within the allowable range. The consistency on the results of carbon steel corrosion test and FEM simulation demonstrates that the integrated multi-physical model is feasible for analyzing the stray current corrosion quantitatively.

VI. CONCLUSION

Based on the actual operating conditions of locomotive in Guangzhou Metro, this paper analyzes the stray current distribution and the corrosion rate of buried metal (e.g. buried pipeline) was calculated based on field measured data. The corrosion platform and simulation model of N20 carbon steel

were built, and the experimental data and simulation data were compared and analyzed.

Summarizing the above, we can get the following conclusions:

1) A simulation model was established to directly evaluate the corrosion of buried pipelines, the distribution of stray current and the corrosion rate of buried pipelines between two subway stations were calculated.

2) The leakage of the stray current reaches a larger value at the positions of the locomotive and substation. Thus, the buried pipeline near the locomotive and substation are more vulnerable to corrosion. The potential of the rail to the surrounding environment is gradually reduced, there are different potential on the position of pipeline.

3) Leakage of stray current affects the buried pipeline potential, and a higher potential causes vulnerability to corrosion. The maximum potential of the buried pipeline occurs at the up-rush current (48s) when the locomotive runs at constant speed. The depth of the buried pipeline affects the corrosion rate of the pipeline. The corrosion is serious when the pipeline is buried at a shallow depth.

4) An electrochemical corrosion test platform was built to test the corrosion rate of N20 carbon steel specimens, and the test results were verified by finite element method. Comparing the simulation and experimental results, the error is within the allowable range, which further proves that the finite element method can be used as an effective method to calculate the mass loss of metal corrosion caused by stray current in the subway.

REFERENCES

[1] T. Chchitd and T. Kulworawanichpong, "Stray current assessment for DC transit systems based on modelling of earthing and bonding," *Elect. Eng.*, vol. 101, no. 1, pp. 81–90, 2019.

[2] S. Memon and P. Fromme, "Stray current simulation models for direct current transit system: An industry perspective," in *Proc. Joint Rail Conf.*, San Jose, CA, USA, 2015, pp. 23–26.

[3] J. G. Yu and C. J. Goodman, "Modelling of rail potential rise and leakage current in DC rail transit systems," in *Proc. IEE Colloq. Stray Current Effects DC Railways Tramways*, 1990, pp. 221–226.

[4] K. Tang, "Stray current induced corrosion of steel fibre reinforced concrete," *Cement Concrete Res.*, vol. 100, pp. 445–456, Oct. 2017.

[5] Z. Chen, D. Koleva, and K. van Breugel, "A review on stray current-induced steel corrosion in infrastructure," *Corrosion Rev.*, vol. 35, no. 6, pp. 397–423, 2017.

[6] S. A. Memon and P. Fromme, "Stray current corrosion and mitigation: A synopsis of the technical methods used in DC transit systems," *IEEE Electrific. Mag.*, vol. 2, no. 3, pp. 22–31, Sep. 2014.

[7] A. Zaboli, B. Vahidi, S. Yousefi, and M. M. Hosseini-Biyouki, "Evaluation and control of stray current in DC-electrified railway systems," *IEEE Trans. Veh. Technol.*, vol. 66, no. 2, pp. 974–980, Feb. 2017.

[8] J. Coves, J. S. Aguilar, and J. Rull-Duran, "Modelled, simulation and design of collecting grid of stray currents in slab track in DC electrified railway systems," in *Proc. IEEE Int. Conf. ESARS-ITEC*, Nov. 2018, pp. 1–7.

[9] Z. C. Cai and H. Cheng, "Evaluation of metro stray current corrosion based on finite element model," *J. Eng.*, vol. 2019, no. 16, pp. 2261–2265, 2019.

[10] A. Ogunsola, L. Sandrolini, and A. Mariscotti, "Evaluation of stray current from a DC-electrified railway with integrated electric–electromechanical modeling and traffic simulation," *IEEE Trans. Ind. Appl.*, vol. 51, no. 6, pp. 5341–5441, Nov./Dec. 2015.

[11] Y.-S. Tzeng and C.-H. Lee, "Analysis of rail potential and stray currents in a direct-current transit system," *IEEE Trans. Power Del.*, vol. 25, no. 3, pp. 1516–1525, Jul. 2010.

[12] M. M. Alamuti, H. Nouri, and S. Jamali, "Effects of earthing systems on stray current for corrosion and safety behaviour in practical metro systems," *IET Elect. Syst. Transp.*, vol. 1, no. 2, pp. 69–79, Jun. 2011.

[13] C. Wang, W. Li, Y. Wang, S. Xu, and M. Fan, "Stray current distributing model in the subway system: A review and outlook," *Int. J. Electrochem. Sci.*, vol. 13, pp. 1700–1727, Feb. 2018.

[14] W. Li, "Stray current corrosion monitoring and protection technology in DC mass transit systems," China Univ. Mining, Xuzhou, China, Tech. Rep., 2014.

[15] A. Cerman, F. Janícek, and M. Kubala, "Resistive-type network model of stray current distribution in railway DC traction system," in *Proc. 16th Int. Sci. Conf. Electr. Power Eng.*, May 2015, pp. 364–368.

[16] S. Jabbehdari and A. Mariscotti, "Distribution of stray current based on 3-dimensional earth model," in *Proc. Int. Conf. Elect. Syst. Aircr., Railway, Ship Propuls. Road Vehicles (ESARS)*, Aachen, Germany, Mar. 2105, pp. 1–6.

[17] J. G. Yu and C. J. Goodman, "Stray curremt design parameters for DC railways," in *Proc. IEEE/ASME Joint Railroad Conf.*, Atlanta, GA, USA, Mar. 1992, pp. 19–28.

[18] C. Pei, S. Zhao, P. Xiao, and Z. Chen, "A modified meander line-coil EMAT design for signal amplitude enhancement," *Sens. Actuators A, Phys.*, vol. 247, pp. 539–546, Aug. 2016.

[19] P. Svoboda and S. Zajaczek, "Simulation of stray currents on single track in MATLAB simulink," in *Proc. 15th Int. Sci. Conf. Electr. Power Eng. (EPE)*, Brno, Czech Republic, May 2014, pp. 609–612.

[20] N. Y. Ru, "Research on modeling method of transformer DC bias caused by metro stray current," in *Proc. Int. Conf. Power Syst. Technol. (POWERCON)*, Guangzhou, China, Nov. 2018, pp. 3834–3839.

[21] A. Dolara, F. Foiadelli, and S. Leva, "Stray current effects mitigation in subway tunnels," *IEEE Trans. Power Del.*, vol. 27, no. 4, pp. 2304–2311, Oct. 2012.

[22] Y. Zhang, Q. Feng, L. Yu, C.-M. L. Wu, S.-P. Ng, and X. Tang, "Numerical modelling of buried pipelines under DC stray current corrosion," *J. Electrochem. Sci. Eng.*, vol. 9, no. 2, pp. 125–134, 2019.

ZHICHAO CAI received the B.Eng. degree in electrical engineering and automation from East China Jiaotong University (ECJTU), Nanchang, China, in 2010, and the Ph.D. degree in electrical engineering from the Hebei University of Technology, Tianjin, China, in 2016. He is currently an Associate Professor with the School of Electrical and Automation Engineering, ECJTU. He is also an Adjunct Researcher with Nondestructive Detection and Monitoring Technology for High Speed Transportation Facilities, Key Laboratory of Ministry of Industry and Information Technology. His research interests include electromagnetic acoustic, non-linear ultrasonic, and electromagnetic acoustic emission.

XIANWEI ZHANG is currently pursuing the master's degree with East China Jiaotong University, China. From 2008 to 2018, he was engaged in subway DC power supply technology related work. His research interests include metro stray current, overhead catenary fault detection, and grounding technology.

HAO CHENG received the master's degree from East China Jiaotong University, China, in 2019. He is currently an Assistant Engineer with State Grid Yingtan Power Supply Company, Jiangxi, China. His research interests include power system protection, smart substation, and grounding technology.